Available online at www.sciencedirect.com
SCIENCE DIRECT
Polymer 46 (2005) 455–470
polymer
www.elsevier.com/locate/polymer

Finite strain response, microstructural evolution and β→α phase transformation of crystalline isotactic polypropylene

Wei Xu[a], David C. Martin[a,b,c], Ellen M. Arruda[a,d,*]

[a]Macromolecular Science and Engineering, University of Michigan, 2541 Chemistry Building, Ann Arbor, MI 48109-1055, USA
[b]Department of Materials Science and Engineering, University of Michigan, H.H. Dow Building, Ann Arbor, MI 48109-2136, USA
[c]Department of Biomedical Engineering, University of Michigan, 1113 C.A. Gerstacker Building, Ann Arbor, MI 48109-2099, USA
[d]Department of Mechanical Engineering University of Michigan, 2250 G.G. Brown, Ann Arbor, MI 48109-2125, USA

Received 9 September 2004; received in revised form 25 October 2004; accepted 26 October 2004
Available online 26 November 2004

Abstract

An experimental study of the finite strain response of annealed α and β crystalline isotactic polypropylene (iPP) was conducted over a range of temperatures (25, 75, 110 and 135 °C) using uniaxial compression tests. Uniaxial compression results indicate nearly identical macroscopic stress vs. strain behavior for α-iPP and for β-iPP to true strains in excess of −1.1 at room temperature despite the different initial morphologies. At larger compressive strains (>1.2), β-iPP shows more rapid strain hardening. The orientation of crystalline planes during straining differs at room temperature from that at high temperature, indicating a change of slip mechanisms as temperature increases. In addition, strain-induced crystallization occurred at the highest temperature examined in α-iPP. A continuous transformation of β crystals to α crystals with inelastic deformation at room temperature was observed and it was facilitated at higher deformation temperatures. Scanning electron microscopy (SEM) observations of deformed β-iPP provide strong evidence that the transformation is achieved via a solid-to-solid mechanism despite the different helical hands in α and β crystal structures. Molecular simulations were used to investigate a conformational defect in the 3_1 helical chains of β-iPP, characterized by a 120° helical jump. The propagation of this conformational defect along molecular chains provides the reversal of helical hand required by the solid-to-solid transformation. The β→α phase transformation in iPP is proposed to be accomplished via a solid transformation that includes slip along β(110) and β(120) planes during shear of the crystal lattice.

Keywords: Finite strain response; β→α Phase transformation; Solid-to-solid transformation

1. Introduction

Isotactic polypropylene (iPP) is a semi-crystalline polymer widely used in industrial and commercial applications. Many aspects of the morphology and mechanical properties of iPP and their relationships have been determined. iPP is polymorphic with three known crystalline phases, monoclinic α, trigonal β and triclinic γ. The iPP chains in the lattices of these three crystalline forms are 3_1 helices with either a right or left helical hand. The setting angles of the helical hand relative to the *a* and *b* crystallographic axes (the azimuthal orientation) also vary for different crystal morphologies. The detailed morphological differences between α and β crystal structures are of critical concern in studies of the deformation mechanisms and the β→α phase transformation. For this reason these two morphologies are reviewed.

The well known α phase is the most stable iPP crystal structure with a density of 0.936 g/cm^3 and melting point of 165 °C [1]. The crystalline structure of α-iPP was first established by Natta and Corridini [2] as monoclinic with lattice constants $a=6.65$ Å, $b=20.56$ Å, $c=6.5$ Å and $\beta=99.6°$. The α crystal structure is characterized by a change in the helical hand and azimuthal orientations of the molecular

* Corresponding author. Tel. +1 734 763 5328; fax: +1 734 647 3170.
E-mail address: arruda@umich.edu (E.M. Arruda).

0032-3861/$ - see front matter © 2004 Elsevier Ltd. All rights reserved.
doi:10.1016/j.polymer.2004.10.084

chains on successive (040) planes. The β phase was first observed by Keith et al. [3]. It is less prevalent and its crystalline structure had been an enigma for more than 35 years partly due to the instability of the β phase when drawn, thus rendering it very difficult to obtain β phase fibers for crystalline structural investigation [4]. This structure was determined to have a trigonal unit cell with lattice constants $a=b=11.01$ Å, $c=6.5$ Å and $\alpha=90°$, $\beta=90°$, $\gamma=60°$, independently by Meille et al. [5] and Lotz et al. [6] in 1994.[1] In contrast to the alternating helical hands in α crystals, all of the chains in a β crystal lattice have the same helical hand, either all left or all right, while the azimuthal orientation of the corner chains differs by ~180° from that of the center chains. The β phase has a density of 0.921 g/cm^3 and a melting point of 155 °C [1]. A significant difference between the α and β crystalline structures is the existence of lamellar branches in α spherulites. The branching lamellae manifest themselves under all crystallization conditions [6,7], which becomes an intrinsic property of the α iPP melt-crystallized form. Being thermodynamically less stable than the α phase, the β phase can only be formed under specific conditions [8–14]. At all temperature ranges, the α phase is nucleated more profusely than β phase while the β phase can be crystallized in the presence of β nucleation agents that can yield β phase percentages as high as 90% [15,16].

The mechanical response, deformation mechanisms and microstructural evolution of α-iPP and β-iPP during inelastic deformation have been subjects of recent studies. Hirsch and Wang [17] investigated the texture evolution during compression of α-iPP with 62% initial crystallinity at high temperatures (135 and 155 °C) and three strain rates (0.1, 1 and 10 s^{-1}) using X-ray diffraction analysis. They found that at both temperatures, the crystallographic planes are oriented by the alignment of the *c* axis normal to the compression axis. This orientation can be achieved by a deformation mechanism in which glide occurs on planes normal to the *b*-axis. They also found strong dependence of texturing on temperature, which indicates that at higher temperature a more selective (planar) glide mechanism exists with a preferred glide plane normal to the crystallographic *b*-axis. Hirsch and Wang thus determined that glide on planes normal to the *b*-axis occurs preferentially at 155 °C but not at 135 °C. Pluta et al. [18] studied the morphology and the development of texture in α-iPP subjected to plane-strain compression. DSC and density measurements both indicate a drop in crystallinity as compression ratio increases. The texture orientation of β iPP has not been observed in the literature because it is not stable during inelastic deformation. Transformation to the α phase or the mesomorphic phase may happen during inelastic deformation of β-iPP [19].

It has been observed that a β→α phase transformation occurs during the plastic deformation of β-iPP. Li and Cheung [20] investigated the crystallinity changes of β nucleated iPP (with initial crystallinities of 36% β and 23% α) using WAXS and DSC over the necking region during tensile tests. They observed a steady and significant phase transformation from the β-phase to α-phase after yielding. Also, they recorded a decrease in overall crystal content with inelastic deformation. Deformation in tension is not uniform, however and possible dilatation due to cavitation can obscure the β→α transformation mechanism. Karger-Kocsis [21] attributed the increase of the toughness of β-iPP to the mechanical stress-induced phase transformation from a less dense β phase to a denser α phase crystalline structure. The exothermic characteristic of this transformation also contributes to the increase in toughness since crack tip blunting and subsequent yielding are favored.

The β→α transformation mechanism is not well understood but a melting and recrystallization theory dominates the literature without any clear physical evidence. Stress-induced polymeric phase transformations can be divided into two categories: solid martensitic-like phase transformations and partial melting-recrystallization processes [22]. The martensitic-like mechanism has been used to describe those cases in which the molecular chains of the initial and final crystalline phases have identical conformations, such as the orthorhombic to monoclinic phase transformation of polyethylene (PE), or when the helical hands of molecular chains are preserved, such as the phase II to phase I transformation of isotactic poly(1-butene) (PBu). It has long been suggested that the reversal of helical hand is indeed an impossible molecular event [22]. The β→α phase transformation of iPP has been assumed to involve melting and recrystallization because of the different arrangements of the chain helical hands in α and β crystals. It is believed that since a solid-to-solid transformation has to involve a 'chain rewinding' process, it would not be possible [11,23,24]. The present work hypothesizes, however that the presence of conformational defects in molecular chains readily reverses the helical hands of iPP chains.

The helical hand reversal accomplished via conformational defects during the phase transformation of polytetrafluoroethylene (PTFE) has been widely studied [25–28]. PTFE is in Phase II below 19 °C and at atmospheric pressure. The unit cell is triclinic and comprised of 54/25 helical chains with opposite hands. Phase transformation from phase II to phase IV occurs when the temperature rises to between 19 and 30 °C. Phase IV exhibits a hexagonal unit cell which is comprised of 15/7 helical chains with identical helical hand. Partial melting is not possible at this transformation temperature. Helical reversals via the motion of conformational defects (helical reversal points) were proposed and thought to be energetically feasible as indicated by modeling results [25,29].

[1] The structure has a hexagonal symmetry and this had at one time led to the assumption of a large hexagonal unit cell which contained nine chains [8].

Stress-induced $\alpha \leftrightarrow \beta$ phase transformation of poly(butylene terephthalate) (PBT) was studied by Dobrovolnay-Marand et al. and found to be accomplished via the change of molecular conformation [30]. In α form, the plane of benzene rings is inclined about 19° to the *c* axis of the unit cell, whereas it is nearly parallel to the *c* axis in β form. The rotation of aliphatic groups about the benzene–carbonyl bonds was shown to be feasible for accomplishing the phase transformation.

A 120° helical jump conformational defect for iPP has been proposed in the literature [31,32,33]. Schaefer et al. [31] have reported 2D solid-state NMR studies on α-iPP and presented evidence of a 120° helical jump, wherein the 3_1 helices appear to execute a 120° rotation about their axes. Rutledge [32] analyzed this 120° helical jump accompanied by a *c*/3 translation using quasi-static methods of molecular modeling and examined the mechanisms for describing the chain jump process in terms of energetic stability and activation barrier. The energy analysis reveals that the excess conformational energy (above that of a perfect iPP 3_1) is minimal when the length of the conformational defect dispirations is 6 repeat units (monomer units). The role of this defect in accommodating the helical hand changes required of a solid-to-solid $\beta \rightarrow \alpha$ phase transformation is developed herein.

SEM has been widely used in the literature to study the spherulitic morphology of iPP. Etched α and β iPP crystals are clearly differentiated using scanning electron microscopy (SEM) because of their different lamellar structures [23,34]. The α spherulites are characterized by an interlocking structure in which secondary lamellae grow during crystallization. This interlocking structure renders the α spherulites almost impenetrable to etchants used to remove the amorphous parts of the specimens for SEM analysis. The β crystals form sheaf-like lamellae clusters, or immature spherulites [35] without secondary lamellae and are easily attacked by etchants. The etched α crystals have a relatively smooth surface whereas β crystals have a rough surface. This difference results in melt-crystallized α crystals having a dark contrast in SEM secondary electron images when the electron beam is perpendicular to the sample surface [23]. The well etched β-iPP crystals appear bright under these SEM conditions. The present study tests the hypothesis that α crystals formed via the $\beta \rightarrow \alpha$ transition arising from a shear transformation rather than melting-recrystallization, are therefore devoid of secondary lamellae, and present a well-etched, bright contrast in SEM.

2. Materials and experiments

2.1. Materials and specimens

The iPP used in this study (melt index 4) was provided in pellet form by the Montell Company. The β nucleating agent, a quinacridone dye with a commercial name Hostaperm Red E3B, was provided by Clariant Corporation.

Pellets of iPP were powdered for compression molding of specimens to minimize the possibility of trapping air bubbles during heat treatment. Cylindrical uniaxial compression α-iPP specimens were made by filling the powder into a 9 mm diameter mold and furnace heating at 165 °C for 4 h, followed by heating at 180 °C for 2 h and then furnace cooling at a rate of −15 °C/h. The β-iPP specimens were made by doping the powder with the β-nucleation agent at a concentration of 300 ppm and then subjecting the material to the same heat treatment as the α-iPP. The processing conditions resulted in α-iPP specimens that were 69% crystalline and β-iPP specimens that were initially 74% β crystals and 5% α crystals. The molded specimens were machined and polished to remove the surface and edge defects. The final uniaxial compression test specimens measured 8.5 mm in diameter and 4.5 mm in height.

2.2. Uniaxial compression tests

An MTS 810 servo-hydraulic test machine was used for the compression tests. The α- and β-iPP specimens were compressed at a constant strain rate of $-0.01\ s^{-1}$ to various strain levels at temperatures ranging from room temperature (25 °C) to 135 °C. For high temperature tests a quad-elliptical radiation furnace (model E4-10 by Radiation Energy Research Inc.) was fitted around the specimen and compression platens. The compliance of the MTS apparatus was determined by compression of the load train without a specimen. The loading compliance was found to fit a bilinear load vs. displacement function and was subtracted from the measured displacement across the load train to obtain the specimen displacement. The system compliance is small and this procedure does not unduly alter the constant strain rate conditions. The system compliance contained hysteresis that was not accounted for when processing the unloading responses; the unloading portion of the curves shown here include some machine compliance. Thus the unloading portion of the curves should not be considered fully accurate and only appear to help identify various tests.

Compliance-corrected load vs. displacement data were converted to true stress vs. true strain data by assuming incompressibility which is strictly valid only in the plastic deformation region. The compressibility associated with the small ($\varepsilon < 0.05$) elastic range is neglected. Previous polymer compression tests [36] were conducted using Teflon sheet as a lubricant between the specimen and the compression platen which provided excellent boundary conditions for obtaining homogenous deformations. Here, Teflon grease was used and excellent results were again obtained.

2.3. Differential scanning calorimetry (DSC)

Differential scanning calorimetry (DSC) measurements

were conducted at 10 °C/min in a TA Instruments model 2910 DSC. 2.5 mg samples were cut from the deformed specimens for use in the DSC analysis. The specimens were scanned from 50 to 200 °C in a nitrogen gas purged chamber. The melting enthalpy was obtained by integration of the under-peak area from 100 to 180 °C for both α- and β-iPP with on-line software from Universal Data Analysis. In the case of partial overlapping of α and β melting peaks, the peaks were separated by an approximate method of Gaussian curve fitting using Origin 6.0 software.

2.4. Wide angle X-ray scattering (WAXS)

A Rotaflex Cu Kα rotating anode diffractometer (λ= 1.5405 Å) was used to perform the X-ray diffraction measurements. Samples were tested on the surface perpendicular to the compression direction. Scanning ranged from 3 to 33° at a scanning rate of 5°/min. The detector and sample rotated simultaneously such that the angle between the beam and the sample surface was the same as the angle between the sample surface and the detector. In this θ/θ mode of operation the diffracting planes were parallel to the sample surface and normal to the compression axis. The increase of a peak intensity with inelastic strain indicates that the normal of the associated crystalline planes rotates towards the compression direction.

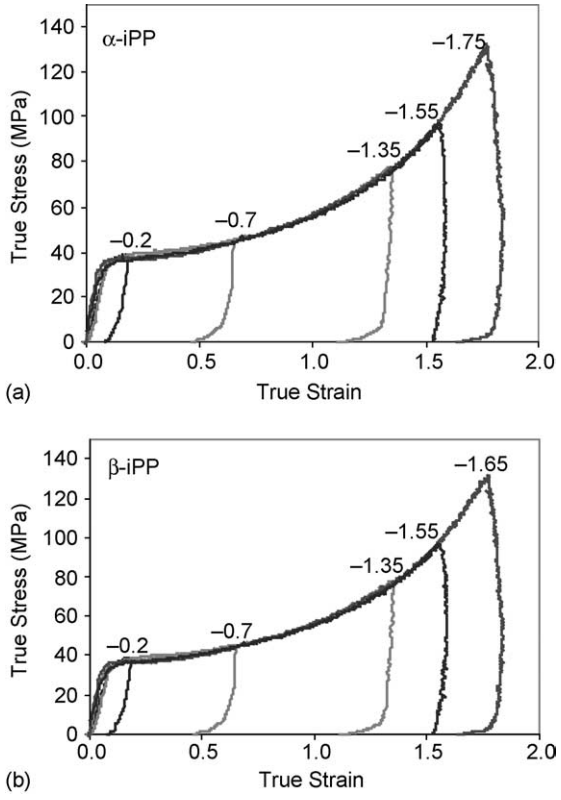

Fig. 1. True stress vs. strain of (a) α-iPP and (b) β-iPP at room temperature (25 °C) to various amounts of strain indicated near each unloading curve (strain rate $-0.01\ s^{-1}$).

2.5. Scanning electron microscopy (SEM)

Undeformed specimens of α- and β-iPP and β-iPP specimens deformed to a final strain of −1.6 at room temperature and 135 °C were used in the SEM examination. The specimens were first polished with fine sandpaper and then carefully polished with 0.1 μm alumina powder until they were smooth and devoid of visible scratches. The specimens were then immersed for 18 h in an acid etchant solution (1.3 wt% $KMnO_4$, 32.9 wt% concentrated H_3PO_4 and 65.8 wt% H_2SO_4) to preferentially etch the amorphous part of the polymer in the spherulites and expose the remaining crystalline lamellar structure. The specimens were washed with hydrogen peroxide (H_2O_2) and acetone subsequently in order to remove any residual etchant. After drying, the specimens were coated with a very thin layer of gold to eliminate any undesirable charging effects during SEM observation. The instrument used in this study was a Philips XL30FEG microscope. The voltage of the electron beam used for SEM observation ranged from 5 to 15 kV. The SEM images were obtained using a secondary electron detector and magnifications ranging from 50 to 10,000×.

3. Results and discussion

3.1. Finite strain response of α- and β-iPP vs. temperature

3.1.1. Isothermal response at room temperature

Fig. 1(a) shows the $-0.01\ s^{-1}$ uniaxial compression response of α-iPP at 25 °C for various final strains. The strains reported are those achieved at the end of loading. The unloading curves demonstrate that the specimens recover a small portion of this deformation on unloading. These curves also demonstrate repeatability of the test procedure and show three characteristic regions on loading: an elastic deformation with a modulus of about 1.45 GPa at the

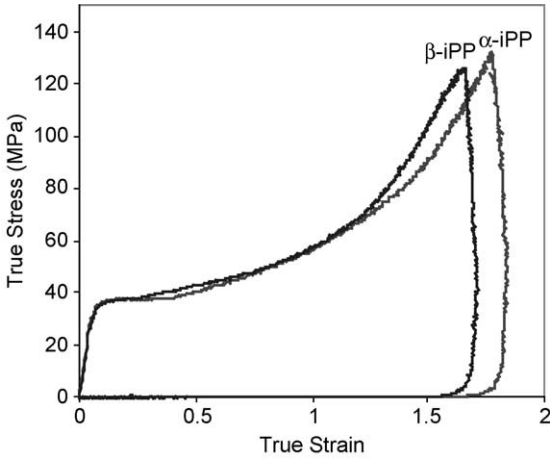

Fig. 2. Comparison of true stress–true strain of α-iPP and β-iPP at $-0.01\ s^{-1}$ and room temperature.

beginning stage of elastic deformation; yield at less than 10% strain followed by an initially low increase in stress with strain after yielding; and a dramatic increase in stress with strain at large strains. Fig. 1(b) contains the $-0.01\ s^{-1}$ uniaxial compression responses of β-iPP at 25 °C for various final strains. The response of β-iPP is very similar to that of α-iPP at this strain rate and temperature. Annealed semi-crystalline iPP shows no true strain softening on yielding in contrast to glassy polymers which soften prior to hardening [35]. The characteristic strain hardening response of glassy polymers is also exhibited here by semi-crystalline iPP. Strain hardening in semi-crystalline polymers involves crystallographic slip mechanisms and crystallographic texturing in addition to amorphous chain orientation. Crystallographic slip in semicrystalline polymers results in less recovery of inelastic deformation as compared to that of glassy polymers.

The large deformation responses of α-iPP and β-iPP are superposed in Fig. 2. The two semi-crystalline morphologies produced via identical heat treatment display remarkably similar initial elastic, yield and strain hardening responses to a compressive true strain of about −1.1. At compressive strains in excess of −1.1, the rate of strain hardening of β-iPP is seen to exceed that of α-iPP. This divergence at large strains is in agreement with the Karger-Kocsis' observation in tension which is attributed to the β→α phase transformation [37]. In contrast to the Karger-Kocsis' observation that β-iPP had a higher initial modulus and yield stress, both iPPs tested here show nearly identical initial moduli and yield stresses. Here the initial β-iPP has a higher overall crystallinity than α-iPP and this may slightly increase the modulus of β-iPP and also raise its yield stress. Since cavitation is suppressed in compression, the higher rate of strain hardening in β-iPP vs. α-iPP is not due to the easier cavitation in α-iPP. One explanation for the higher strain hardening rate in β-iPP is that the β crystal are less constrained from deformation since they do not have interlocking secondary lamellae, this results in the commencement of orientation hardening of amorphous regions and crystallographic texturing at lower strains in β crystals and is consistent with the observation of Aboulfaraj et al. [34].

3.1.2. Temperature dependent response

The temperature dependent response of α-iPP and β-iPP can be examined using isothermal testing at a constant strain rate of $-0.01\ s^{-1}$. Fig. 3 contains the temperature dependent stress–strain response of α-iPP and β-iPP. As temperature increases, both morphologies show decreases in modulus and yield stress, which are typical of

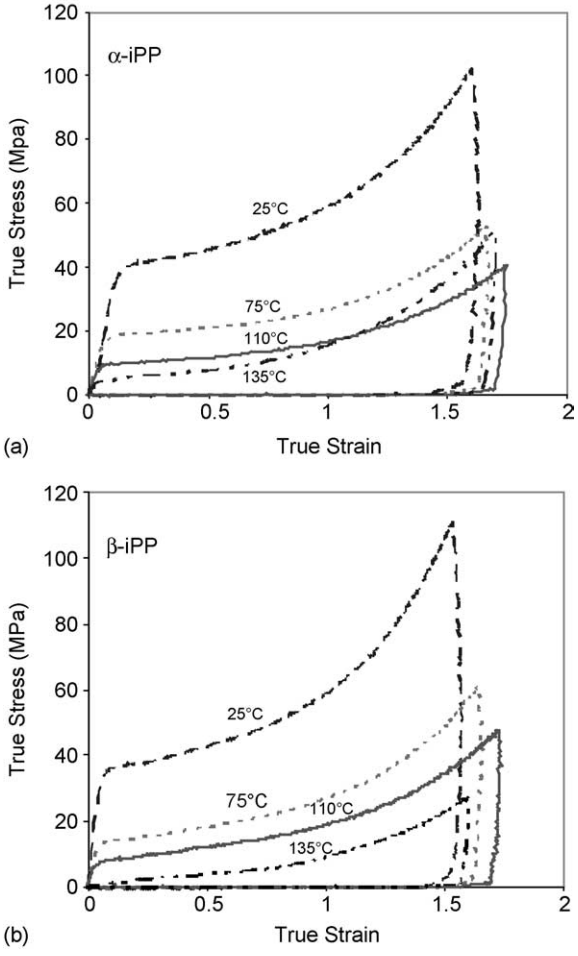

Fig. 3. True stress vs. strain of (a) α-iPP and (b) β-iPP at $-0.01\ s^{-1}$ vs. temperature.

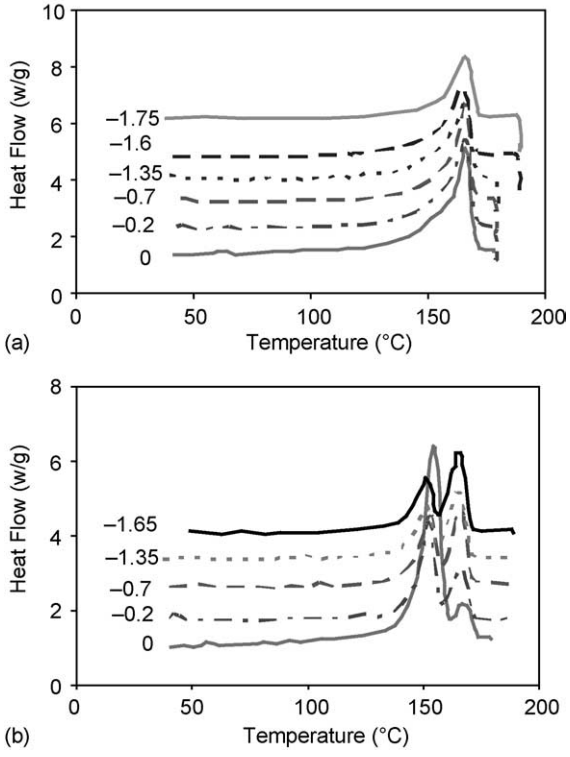

Fig. 4. DSC traces of (a) α-iPP and (b) β-iPP vs. inelastic deformation (strain rate $-0.01\ s^{-1}$ and room temperature (25 °C)).

thermoplastics. The strain hardening rate also decreases with increasing temperature for both morphologies. This has previously been observed in glassy polymers and attributed to a thermally equilibrated entanglement network [38]. In semi-crystalline iPP, changes in the crystal content with temperature and deformation as well as temperature sensitive slip resistance may be contributing to the temperature dependent strain hardening as well.

If the stress–strain responses of α-iPP and β-iPP were superposed, the similarity of the mechanical response of α-iPP and β-iPP would be seen at all temperatures tested at true strains up to about −1.0. At larger compressive strains, β-iPP shows more strain hardening than α-iPP at all temperatures except at 135 °C. The strain hardening rate of α-iPP at 135 °C is higher than that at 110 and 75 °C after true strains of −1.2. This is likely to be due to strain-induced crystallization in α-iPP at 135 °C as will be demonstrated via DSC in the next section.

3.2. Microstructural evolution of α- and β-iPP during plastic deformation

3.2.1. Microstructural evolution at room temperature

Fig. 4(a) shows the DSC traces from undeformed α-iPP and from α-iPP samples after plastic deformation at $-0.01\ s^{-1}$ and room temperature to strains of −0.2, −0.7, −1.35, −1.65 and −1.75. The endotherm at 165 °C indicates melting of the α crystals. Integration of the endotherm area yields an estimate of the percent crystallinity of α crystals. The undeformed sample shows the largest endotherm area. As α-iPP is plastically deformed the area under the endotherm decreases indicating a loss in crystallinity of α-iPP. We have recently shown a similar continuous change in crystallinity with inelastic deformation in quenched α-iPP [39]. More recently Pluta et al. also reported a loss in crystallinity in α-iPP during plane strain compression [18]. Fig. 4(b) shows the DSC traces from undeformed β-iPP and from β-iPP samples after plastic deformation to strains of −0.2, −0.7, −1.35 and −1.65. The undeformed sample is mostly β crystals as evidenced by the strong endotherm at 155 °C, the β melting temperature. A small percentage (5%) of α crystals exists initially as well. It can be seen in Fig. 4(b) that during inelastic deformation the endotherm peak of the β crystalline phase decreases and that of the α crystalline phase increases, indicating a continuous transformation of β crystals to α crystals with inelastic deformation. The DSC trace of undeformed α-iPP shows a barely perceptible shoulder from the melting of β crystals. As the α-iPP is deformed, the shoulder disappears, also indicating a transformation of β phase to α phase during plastic deformation.

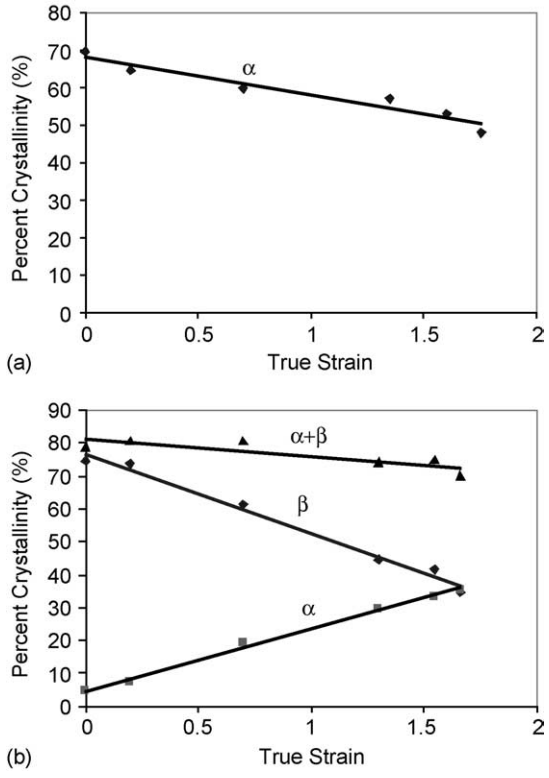

Fig. 5. Percent crystallinity of (a) α-iPP and (b) β-iPP vs. inelastic deformation (strain rate $-0.01\ s^{-1}$ and room temperature (25 °C)).

Fig. 5(a) shows the change of percent crystallinity vs. true strain of α-iPP computed from the endotherms in Fig. 4(a). The initial crystallinity is 69%. During inelastic deformation to a strain of −1.75, the crystallinity of α-iPP drops significantly from 69 to 48%. An initial drop in crystallinity can be seen to occur by 20% strain, i.e. soon after plastic deformation commences. The drop in crystallinity of α-iPP during deformation is coincident with an early study by Lima et al. [40], in which plane strain compression was employed. The significant decrease in crystallinity is due to a first-order phase transformation, i.e. amorphization due to large plastic deformation. As can be seen in Fig. 4(a), the onset of the α phase melting peak shifts to higher temperature with the increase in true strain. For the undeformed specimen, the onset is at about 70 °C, while for the specimen deformed to a true strain of −1.75, it is at about 110 °C. This is evidence of the destruction of small sized crystallites during deformation, which results in the overall crystallinity drop seen in Fig. 5(a).

Fig. 5(b) shows the crystallinity changes of both the α and β phases in β-iPP vs. true strain which were also obtained from integration of the endothermal peaks. The undeformed β-iPP contains 74% β crystals and 5% α crystals. The crystallinity of the β phase decreases by 40% during inelastic deformation to a strain of −1.65. Concurrently the α crystallinity increases by 31%. This is in contrast to the α crystal content lost during deformation when β crystals are not present. The β→α transformation occurs at a practically constant rate with inelastic straining; however, the loss in β crystallinity occurs at a slightly faster rate than the increase in α crystals. As a result, the overall

crystallinity drops by 8.8%. These results are in agreement with a previous study by Li and Cheung [20] over the necking region of β-iPP during tensile tests. However, their results show a rapid phase transformation at the early stage of deformation (true strain less than 100%), followed by a relatively smooth rate of phase transformation. In our study, the rate of phase transformation is almost constant. The current results are from homogeneous, constant strain rate compression tests and may be considered indicative of the actual material response unencumbered by the geometric instability, strain and strain rate gradients characteristic of the tension test.

Fig. 6 contains the WAXS results for the same series of α-iPP and β-iPP samples reported in Fig. 4. The important characteristic scattering peaks of the α phase can be found at scattering angles 2θ of 14° (110), 17° (040), 18.5° (130), 21° (111) and 22° ($\bar{1}$31) and (041) and the β phase peaks can be found at 16° (110) and 21° (111). For the WAXS experiments described earlier, only the crystalline planes parallel to the sample surface were sampled. The increase of a peak intensity with deformation indicated the orientation of the corresponding plane normals toward the compression axis such that the planes themselves tended to align parallel to the flow direction. The decrease of a peak intensity means that the corresponding planes rotated such that they are aligned parallel to the compressive axis. As inelastic deformation of α-iPP increased, Fig. 6(a) shows that the intensities of the 21 and 22° peaks gradually became dominant, which indicates that the (111) planes and either ($\bar{1}$31) or (041) planes (or both) have been preferentially oriented parallel to the sample surface. The intensity of the 14° peak drops dramatically with deformation indicating the (110) planes rotated such that their normals tended to align towards the flow direction. The WAXS of the undeformed sample (strain 0.0) shows the existence of a small amount of β phase indicated by the small peak at 16° ((110) β planes). As plastic deformation occurred, this peak disappeared

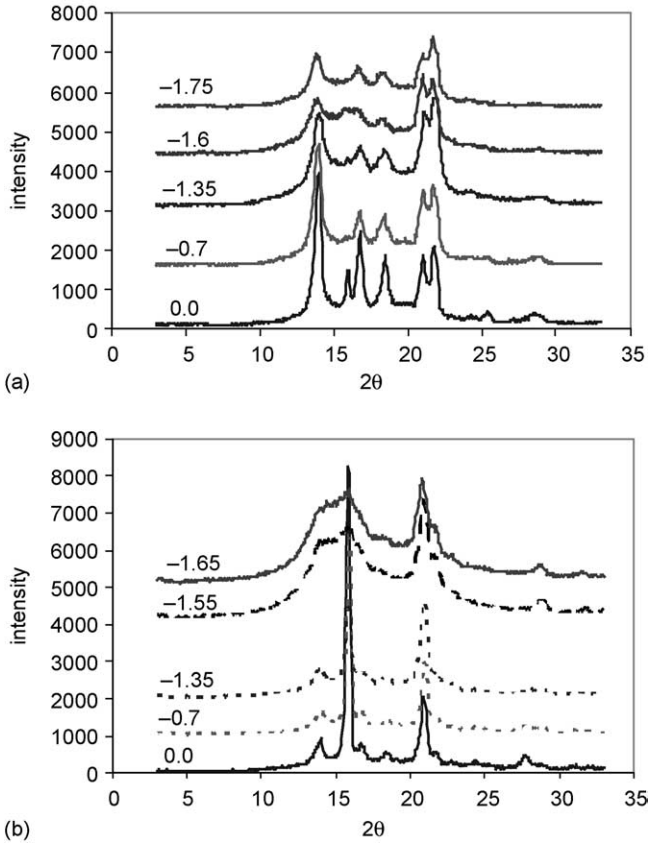

Fig. 6. WAXS of (a) α-iPP and (b) β-iPP vs. inelastic deformation (strain rate $-0.01\ s^{-1}$ and room temperature (25 °C)).

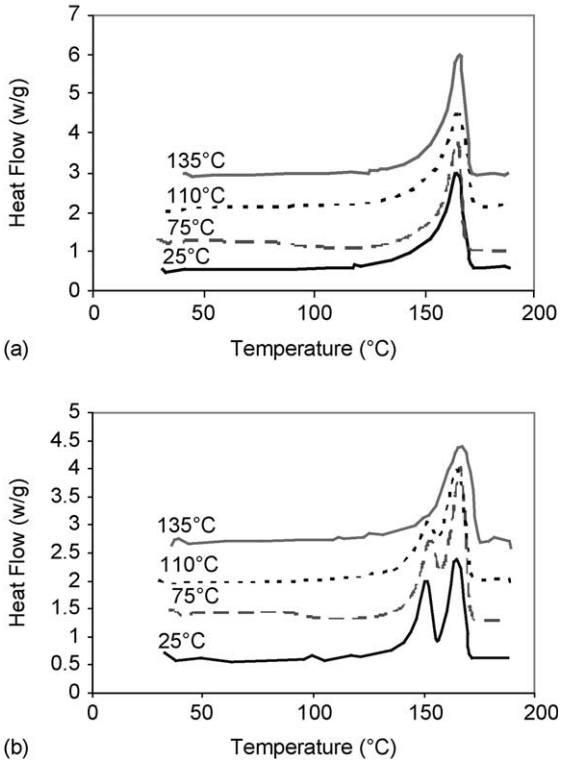

Fig. 7. DSC traces of (a) α-iPP and (b) β-iPP after deformation to true strain of -1.60 at $-0.01\ s^{-1}$ vs. temperature.

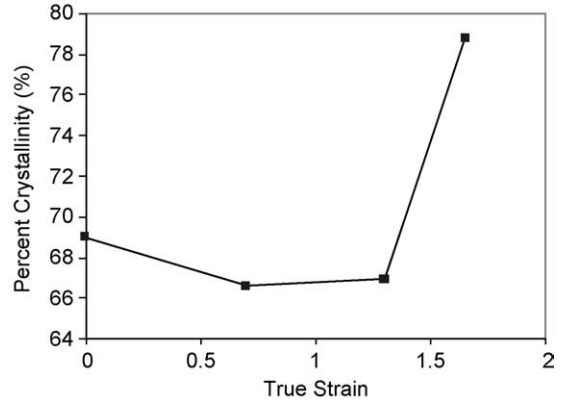

Fig. 8. Crystallinity of α-iPP vs. true strain at 135 °C.

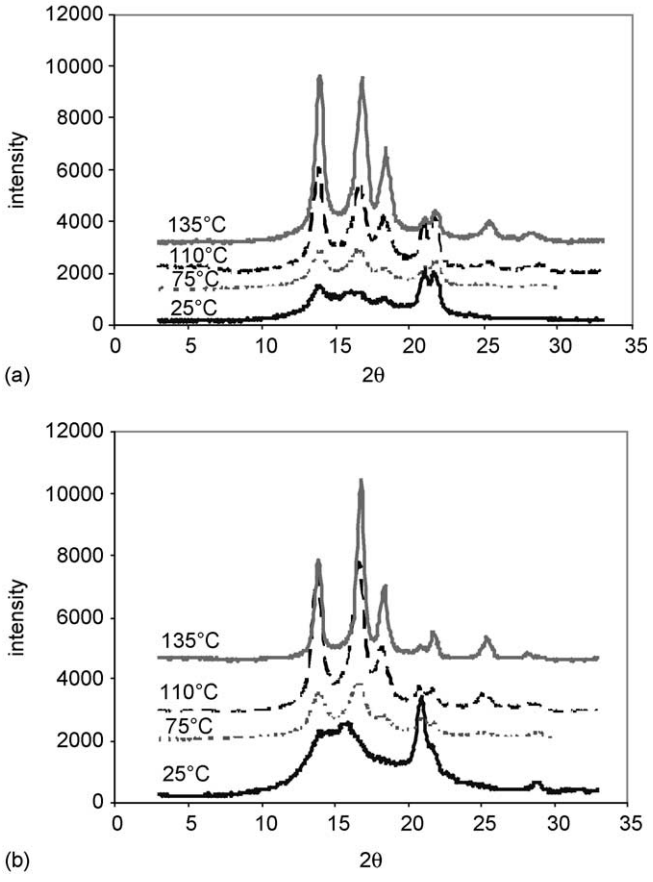

Fig. 9. WAXS of (a) α-iPP and (b) β-iPP after deformation to true strain of −1.60 at $-0.01\ s^{-1}$ vs. temperature.

indicating that the β phase transformed or the (110) β plane normals rotated towards the flow direction. The absence of the β shoulder in the DSC traces of deformed α-iPP in Fig. 4(a) confirms the former. It can also be seen in Fig. 4(a) that the scattering peaks of α crystals become broader with the increase of true strain. This may indicate a decrease in the average crystallite size, the introduction of defects within the crystal or broadening of the d-spacing distribution by deformation of crystals.

Fig. 6(b) shows the WAXS results for the series of β-iPP samples reported in Fig. 4(b). From these curves, evidence of the β→α phase transformation during inelastic deformation can be readily observed. However, interpretation of texture for β crystals is somewhat obscured by this phase transformation. The growth of the 14° peak intensity provides strong evidence of the increase of the α phase. This intensity could also grow if existing α (110) planes rotated towards the flow direction with no net increase in α crystallinity, but such texturing is in contrast to the α-iPP texturing indicated in Fig. 6(a) in which α (110) planes rotated away from the flow direction.

The drop of the 16° peak intensity can be caused by either the decrease of the percentage of the β phase, the rotation of β (110) planes away from the flow direction, or both. Further analysis of the texturing during deformation of β-iPP is complicated by the β→α transformation. The 21° peak, for instance, is a combination of both (111) planes of the α phase and (111) planes of the β phase. This peak would increase for α(111) planes orienting parallel to the sample surface. It can also be expected that this peak intensity will drop as the β phase percentage decreases and increase as the α phase percentage increases. It is therefore quite difficult to unambiguously separate texture effects from the change in α content with deformation.

The WAXS patterns of deformed α- and β-iPP beyond a true strain of −1.55 both show broad peaks at 15° and 21.5°. This could be evidence of the appearance of the mesomorphic phase during large plastic deformation. However, according to Wang et al. [41], the mesomorphic phase should have a small endothermal peak around 58 °C followed by an exothermal around 96° on the DSC trace, which represents chain reorganization (or 'melting') of the mesomorphic phase and its recrystallization process. The DSC traces of α- and β-iPP at large deformation (Fig. 4) do not have these characteristic peaks, so the broad peaks on WAXS are assumed to be due to the increase of the amorphous halo.

3.2.2. Temperature dependence of microstructural evolution

Fig. 7 shows the DSC traces of the specimens after deformation at different temperatures to a final strain of −1.60 at a strain rate of $-0.01\ s^{-1}$ for both the α- and β-iPP. Both morphologies show a temperature dependent crystal content after deformation. In Fig. 7(a), the melting peaks of the α-iPP deformed between 25 and 110 °C do not change significantly with temperature, while the melting peak of the specimen deformed at 135 °C is large, indicating a greater final crystallinity. Table 1 contains the crystallinities calculated from the DSC traces in Fig. 7(a). The crystallinity before deformation is 69%. As the deformation temperature ranges from 25 to 110 °C, the crystallinity at a final strain of −1.60 increases slightly from 53 to 59%. At 135 °C the remaining α-iPP crystallinity increases to 79%. To show that this is not the result of aging at 135 °C and is in fact the result of strain-induced crystallization at this temperature, the change in crystallinity of α-iPP during deformation at 135 °C was monitored at various strain levels. As shown in

Table 1
Percent crystallinity of α-iPP after deformation to $\varepsilon = -1.6$ at different temperatures (the initial crystallinity was 69%)

Deformation temperature (°C)	25	75	110	135
Percent crystallinity (%)	53	58	59	79

Table 2
Percent crystallinity of β-iPP after deformation to $\varepsilon = -1.6$ at different temperatures (the initial crystallinity was 74% β+5% α)

Deformation temperature (°C)		25	75	110	135
Percent crystallinity (%)	α phase	33	43	52	61
	β phase	41	29	22	5
	Total (α+β)	73	72	74	66

Fig. 8, the crystallinity of α-iPP initially decreases with plastic deformation and then increases rapidly as the strain exceeds −1.3, indicating strain-induced crystallization at this high temperature.

Fig. 7(b) clearly shows that as the deformation temperature of β-iPP increases, the β melting peak decreases and the α melting peak increases, indicating that the β→α phase transformation is favored by higher deformation temperatures. Table 2 contains the calculated crystallinity from Fig. 7(b), which shows the amounts of the remaining α, β and total crystalline phases after deformation. At 135 °C, the β crystals have almost completely transformed to α crystals; less than 5% remain. The overall crystal content is not preserved during the transformation and at the highest temperature tested, in which the transformation is practically complete, overall the crystallinity is reduced during inelastic deformation by 13%.

Fig. 9(a) and (b) contain the WAXS results for the α-iPP and β-iPP specimens deformed at different temperatures. In α-iPP it can be seen that as temperature increases, the intensities of the α(110) 14° and α(040) 17° peaks become dominant. The WAXS patterns at 135 °C are consistent with those of Hirsch and Wang who attributed the pattern to slip with more than one active, or preferential, system [17]. Fig. 8 demonstrates that the texture in Fig. 9 is actually largely the result of a 12% increase in crystallinity during the later stages of straining due to strain-induced crystallization of α crystals. At large strains the amorphous chains in iPP are aligned parallel to the flow direction. Strain-induced crystallization results in crystals whose chain direction is

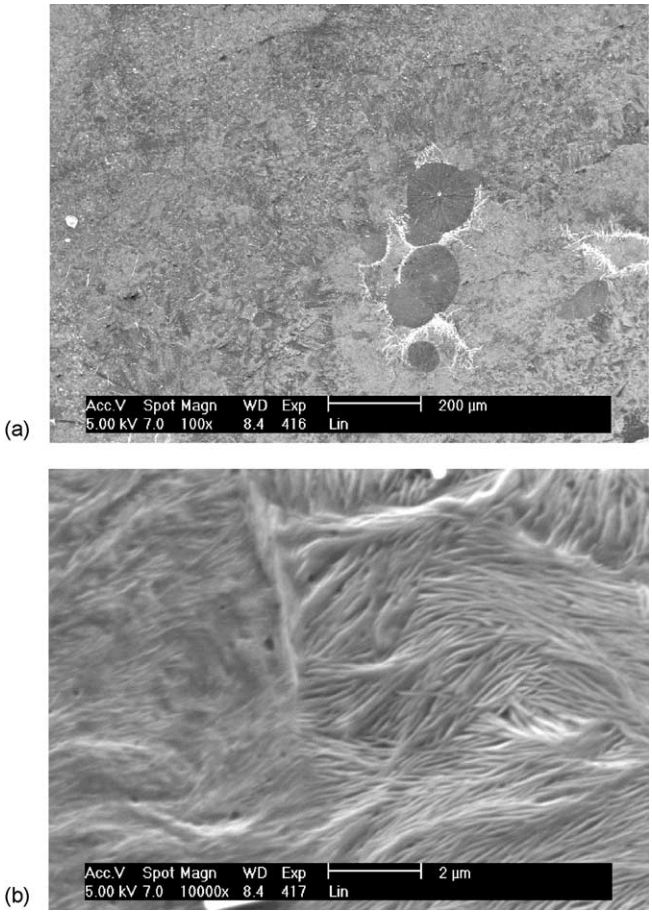

Fig. 10. SEM of undeformed β-iPP at different scales.

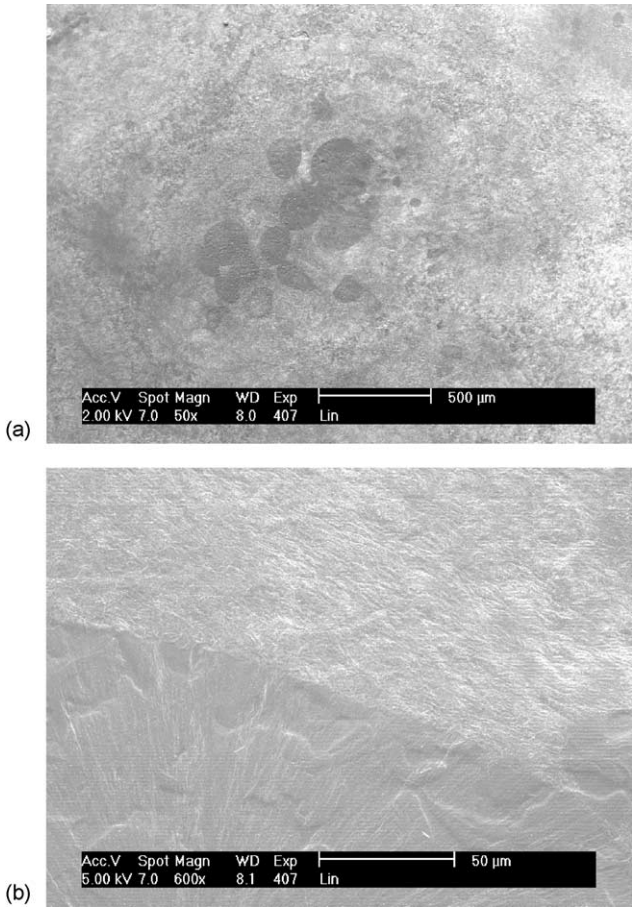

Fig. 11. SEM of deformed β-iPP to a final strain of −1.6 at room temperature at different scales.

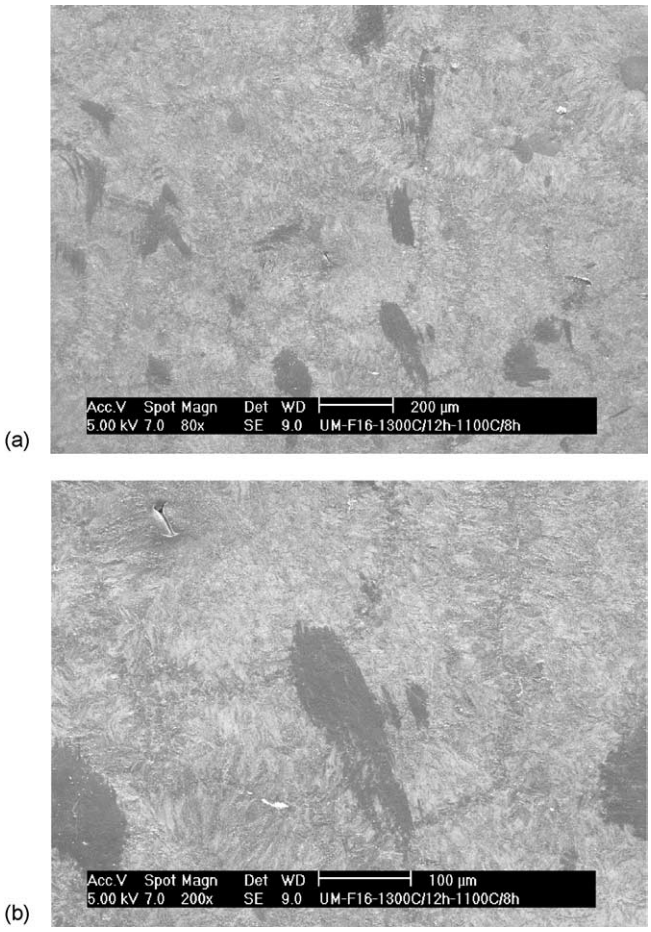

Fig. 12. SEM of deformed β-iPP to a final strain of −1.6 at 135 °C at different scales.

along the flow direction. The WAXS pattern at 135 °C is consistent with strain-induced crystallization as peaks corresponding to planes parallel to the chain axis [(110), (040) and (130)] are all prominent.

The WAXS patterns at intermediate temperatures, for which strain-induced crystallization was not observed, show an orientation of (040) planes towards the flow direction, indicating preferential slip on (040) planes. This texture is in contrast to the low temperature results at 25 and 75 °C in which (111) and ($\bar{1}$31) and/or (041) planes rotate towards the flow direction. This temperature variation of the texturing could be the result of either a change of active slip systems or the change of slip mechanism from coarse slip to fine slip as temperature changes from low to high [42].

In β-iPP at high temperatures the WAXS patterns of Fig. 9(b) show the disappearance of the pure β peak (110) at 16° even though a substantial amount of β crystals remain at the end of the deformation at 75 and 110 °C. These results may provide evidence that the (110) β planes rotate away from the flow direction during deformation. At the highest temperature tested (135 °C), the microstructure is almost fully α-iPP by the end of deformation. The WAXS pattern shows strong alignment of (040) planes with the flow direction.

3.3. SEM investigation of the mechanism of β→α phase transformation

As mentioned earlier, being an intrinsic characteristic of melt-crystallized α crystals, the interlocking structure of α spherulites forms under nearly any crystallization conditions [6,8]. It can then be assumed that if α crystals result from melting and recrystallization during the β→α phase transformation, they would have the interlocking structure. In contrast, if the phase transformation mechanism is a solid-state transformation process, involving shear of β crystals and no melting and recrystallization, the resulting α crystals would not develop the interlocking structure and would etch similarly to, and appear as, β crystals in the SEM.

Fig. 10 shows SEM images of undeformed β-iPP at different magnifications. Fig. 10(a) shows a few dark α spherulites in a bright background of β lamellar clusters. Fig. 10(b) is a boundary region of α and β crystals and the lamellae of both α and β crystals can been clearly observed.

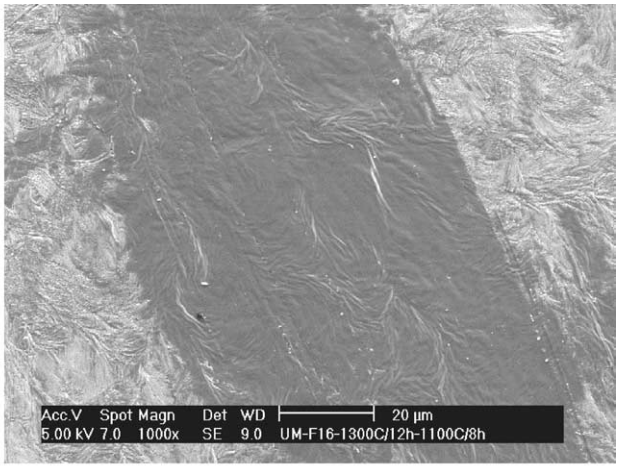

(c)

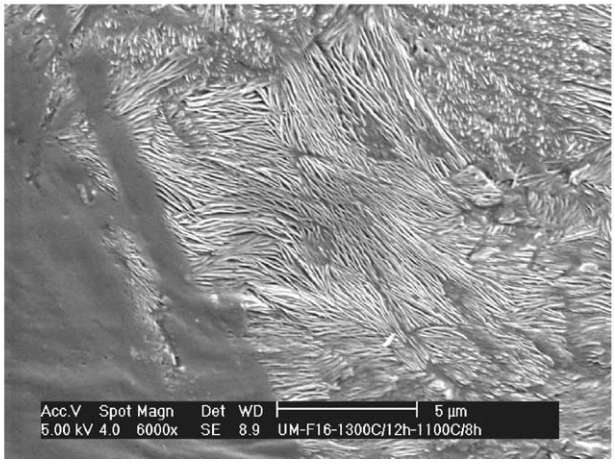

(d)

Fig. 12 (*continued*)

The lamellae of α crystals are straight and the secondary lamellae can also be observed. The lamellae of β crystals are curved and twisted as is clearly shown in Fig. 10(b).

Fig. 11 shows SEM images of β-iPP deformed to a final strain of −1.6 at room temperature. DSC and WAXS studies show that roughly half of the β crystals have transformed to α crystals. The SEM images of Fig. 11(a) show mostly bright crystals with the existence of a few dark α spherulites. The conclusion is that the transformed α crystals still look like β crystals in the SEM, the etchant has penetrated the α crystals, and they lack the interlocking secondary lamella. There is no evidence of a majority of recrystallized α crystals as a result of phase transformation. Fig. 11(b) is a boundary of a bright region and a dark region, where it can be clearly seen that the bright region does have lamellar structures and it is a crystalline region. Thus the deformation of β-iPP at room temperature resulted in α crystals that do not have the secondary lamellar morphology characteristic of melt-crystallized α crystals.

The evidence of a solid-to-solid phase transformation is clearer in SEM images of β-iPP specimens deformed to a final strain of −1.60 at 135 °C, as shown for example in Fig. 12. DSC and WAXS investigations show that almost all of the β crystals have transformed to α crystals at this stage. Again, SEM images show that most of the region is bright, which is the typical presentation of β crystals. Some deformed α spherulites can also be seen. Lamellar structures of both α and β crystals can be clearly observed in the close-up image in Fig. 12(c) and (d). The lamellae in the bright region do not have secondary lamellae, which is again evidence that no melting and recrystallization process was involved in the β→α phase transformation.

These SEM observations clearly show that there are no epitaxially grown secondary lamellae in the transformed α crystals. No melting and recrystallization process occurred to any large extent during the β→α phase transformation. Instead, a solid-to-solid transformation process dominated the transition.

3.4. A mechanism for the solid-to-solid phase transformation

The SEM observations provide evidence that the β→α phase transformation involves the solid transition of β

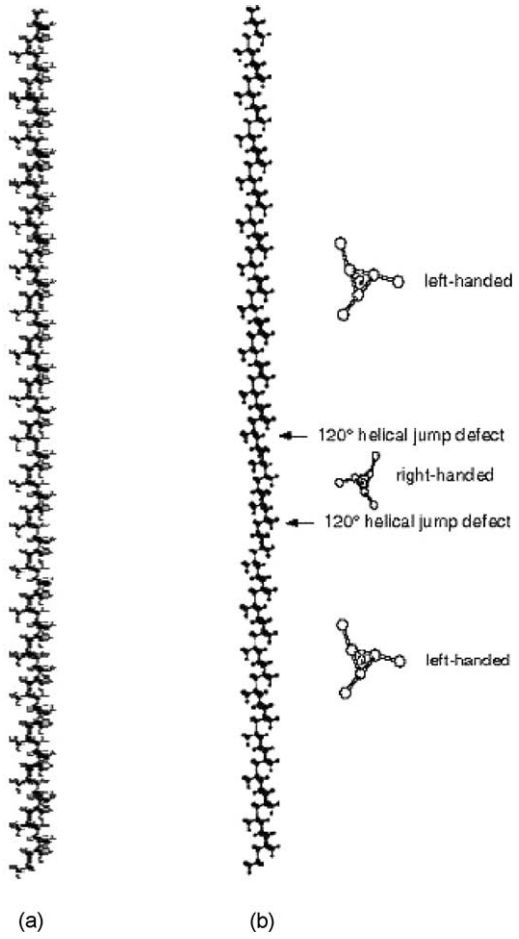

Fig. 13. Molecular chain simulation of (a) perfect 3_1 iPP helix, (b) 3_1 iPP helix with two 120° helical jumps at the central position; the helical hand changes at every helical jump; propagation of the defect along the chain will reverse the helical hand (generated with Cerius2).

crystals to α crystals. The problem remains to describe how the common helical hands in β crystals may transform to the alternating helical hands of α crystals in a solid state. In this section a molecular simulation is presented of the accommodation of 120° helical jump conformational defects in β crystals and their role in the reversal of helical hand. A solid phase transformation mechanism is presented.

A conformational defect that has been postulated to occur in iPP crystals is a 120° helical jump dispiration along the chain, as simulated in Fig. 13 using Cerius[2] software. This helical jump defect along a molecular chain changes the helical hand of the chain such that the helical hand differs on either side of the defect. Fig. 13(a) is an image of a left-handed 3_1 helical iPP molecular chain generated with Cerius[2] molecular simulation software. Composed of 60 (20×3) repeats units (20 times of the β lattice constant c), the chain has a length of 130 Å, which is on the order of the thickness of iPP lamellae. Two 120° helical jump defects have been inserted near the central position of the chain in Fig. 13(b). The first defect changes the helical hand from left-handed to right-handed and the second changes it back to left-handed. As the helical jumps propagate along the molecular chain away from the center, the left-handed chain helix reverses and becomes right-handed. Energy calculations reveal that the total energy rises by 17.4 kcal/mol as the result of the insertion of the conformational defects. The increase of energy mainly comes from bond stretching (4.3 kcal/mol), bond torsion (8.7 kcal/mol) and angle bending (10.0 kcal/mol). However, the van der Waals energy drops by 7.9 kcal/mol.

Fig. 14(a) shows the superlattice of β crystals with the defective chain of Fig. 13(b) inserted at the left bottom corner, replacing a perfect chain. The superlattice is made of 320 β unit cells (4×4×20) by stacking 20 units cells along the *c* crystallographic axis, 4 along the *a* axis and 4 along the *b* axis. Dreiding force field [43] (Dreiding 2.2.1) has been applied for energy minimization. Energy calculations show that the insertion of the conformationally defective chain results in an energy increase of 155.5 kcal/mol. The energy increase can be subdivided to two contributions, the intramolecular distortion and the intermolecular packing interaction. The intramolecular distortion includes bond stretching, angle bending and bond torsion. The intermolecular packing interaction includes van der Waals energy and electrostatic energy. Energy calculation reveals that the energy increase of the defective superlattice is mainly caused by the increase of van der Waals energy (128.0 kcal/mol) and electrostatic energy (32.0 kcal/mol). The intermolecular distortion energy actually drops by 4.6 kcal/mol. If more defective chains are inserted in the superlattice, the extra energy needed to accommodate these defective chains should also increase. Table 3 shows the total energy and energy increase of the 4×4×20 superlattice with 1, 4 and 16 defective chains. It should also be noted here that the defective chain is only modeled at one of the three non-equivalent positions in the β crystal lattice and that these would be expected to yield somewhat different energy increases. The β crystal lattice is shown in Fig. 15(a) in which the presence of 120° helical jump defects and their propagation is assumed to result in the alternating helical hand structure. A solid-to-solid phase transformation that

Table 3
Energy increase as the result of defect chains in the 4×4×20 superlattice

4×4×20 Superlattice	Perfect	1 Defect chain	4 Defect chains	16 Defect chains
Total energy (kcal/mol)	−7944.63	−7789.15	−7374.06	−6404.36
Energy increase (kcal/mol)	–	155.48	570.57	1540.27

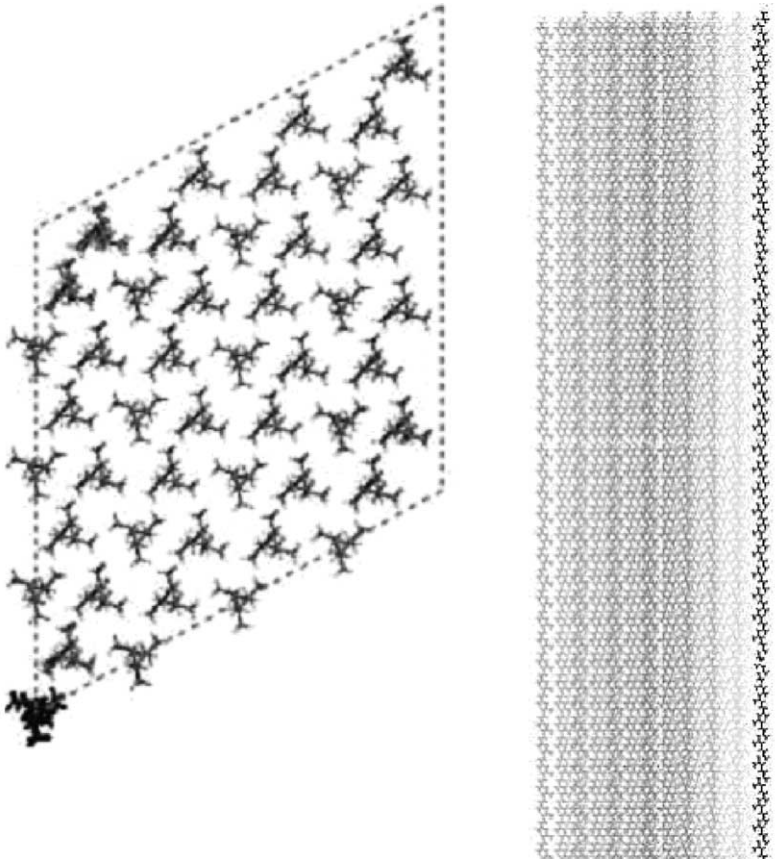

Fig. 14. Molecular simulation of the β crystal superlattice (a) view on (001) plane, the defect chain is at the left bottom corner and (b) view on (110) plane, the defect chain is on the far right side and is highlighted (generated with Cerius2).

can occur simply via crystalline plane slip and lattice shear. When the specimen is plastically deformed, transverse partial slip on β(110) planes occurs and the intermediate structure shown is obtained. From this configuration a shear deformation of the intermediate lattice results in the α crystal, as shown in Fig. 15(b). In Fig. 16, the process is sketched for slip on β(120) planes. This slip during shear process results in a continuous β→α transformation. The 3D deformation gradient **F** is calculated for the transition involving slip on both sets of planes using the unit cell dimensions before and after the deformation; these are given in Fig. 15(b) and Fig. 16. The volume change after the transformation in both cases can be estimated by calculating the determinant of the deformation gradient **F**. The ratio of volumes after and before transformation is 0.9832 and 0.9815 for Figs. 15 and 16, respectively. Both of these are very close to the density ratio of β and α crystals, 0.9840.

4. Conclusions

The true stress vs. true strain responses of α-iPP and β-iPP were examined via uniaxial compression over a range of strain rates and temperatures. The evolution of microstructure with plastic deformation was examined via DSC and WAXS analysis. WAXS results indicated an increased orientation of α(111) planes normal to the compression direction at low temperature (25 °C), with α(040) planes oriented instead at high temperatures (110 and 135 °C). At the highest temperature tested (135 °C), strain-induced crystallization occurred at large compressive strains which was manifested in the WAXS by the prominence of peaks associated with planes parallel to the chain axis. The sudden increase in α crystallinity associated with strain-induced crystallization at 135 °C was also seen via DSC. DSC and WAXS results clearly showed the β→α phase transformation during compression of β-iPP. WAXS indicated that α crystals formed such that α(111) planes oriented normal to the compression direction during the transformation at room temperature tests. At high temperatures α(040) and α(130) planes oriented normal to the compression direction. SEM was used to observe the morphology of undeformed and deformed β-iPP and provide strong evidence for a solid-to-solid phase transformation process.

Deformed β-iPP, which was shown by DSC and WAXS analysis to contain 33% α and 41% β crystallinity at room temperature and 61% α and 5% β at

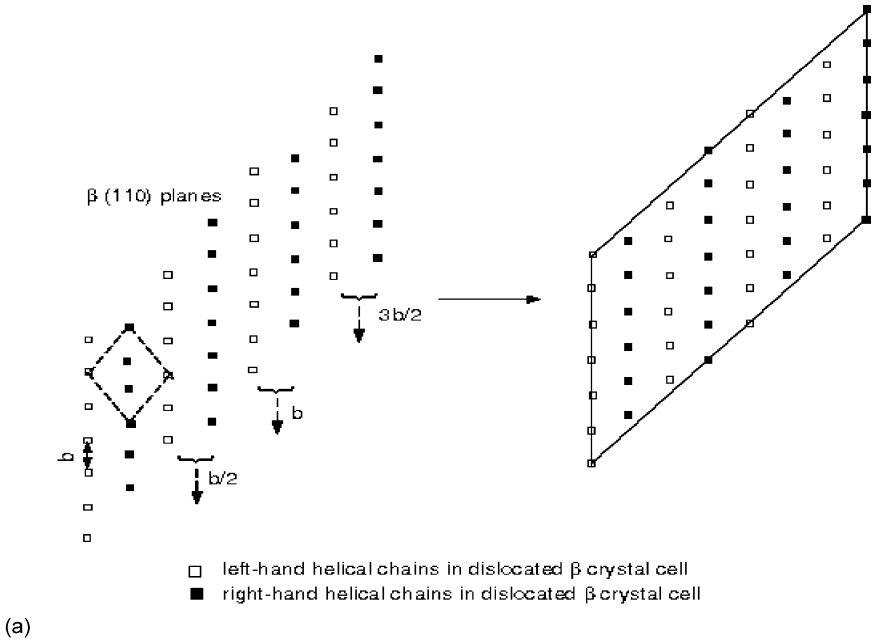

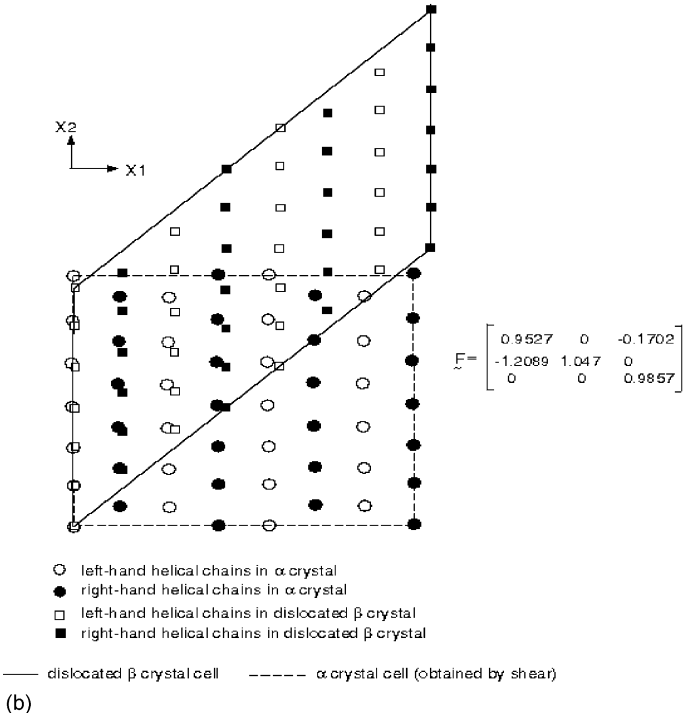

Fig. 15. Illustration of the β (110) slip during shear model for the β→α transformation.

135 °C, exhibited α crystals in SEM that were without secondary lamellae and therefore not the result of melt-recrystallization. These micrographs conclusively demonstrate that the β→α phase transformation is the result of a solid-to-solid phase transformation mechanism. This result is the first example of a solid polyolefin phase transition involving chain reversal. Molecular simulations were conducted to provide a mechanism for the conformational change by simulating the β crystalline lattice containing molecular chains with 120° helical jump conformational defects. The propagation of these defects along the chains can reverse the helical hand of molecular chains in the solid state. A solid-to-solid phase transformation is therefore shown to be accomplished via a simultaneous solid transformation that contains a process of slip along β(110) and β(120) planes and shear of the crystal lattice in the presence of conformational defects. The volume change associated with this

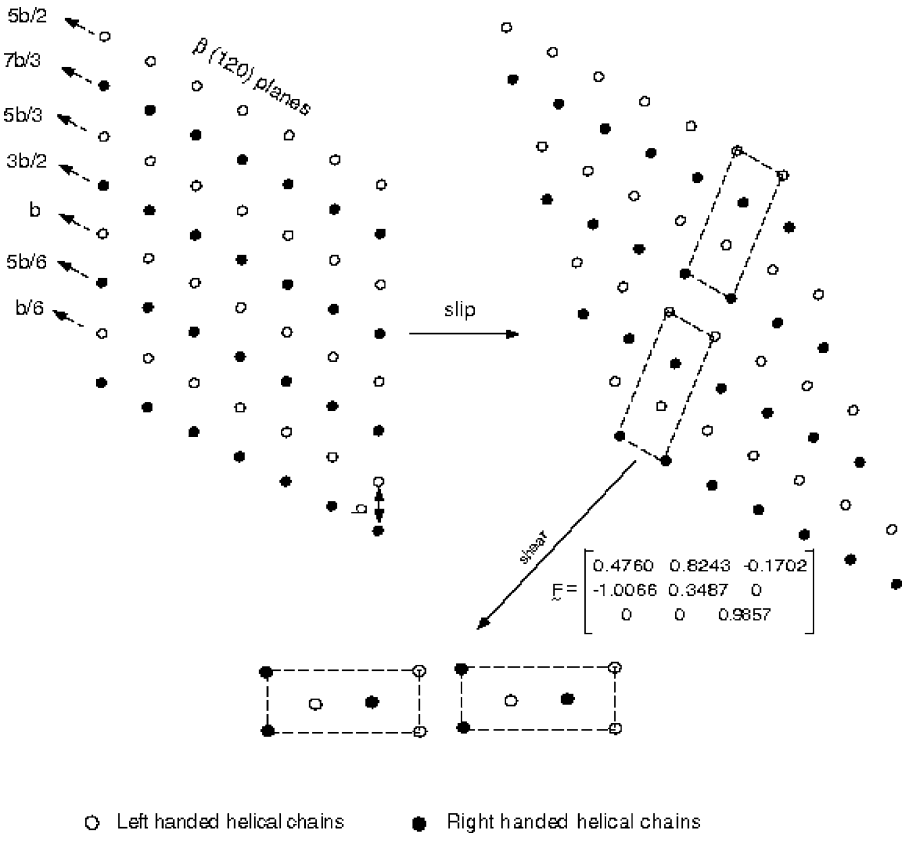

Fig. 16. Illustration of the β (120) slip during shear model for the β→α transformation.

transformation was determined from the deformation gradient tensor **F**, and this accurately matches the known β/α ratio.

Acknowledgements

The support from the US NSF grants No. CMS-9702884 is gratefully acknowledged by EMA. DCM also thanks the support of the NSF through grant no. DMR-0084304.

References

[1] Brandrup J, Immergut EH. Polymer handbook. 3rd ed. New York: Wiley; 1989.
[2] Natta G, Corridini P. Nuovo Cimento Suppl 1960;15:40–51.
[3] Keith HD, Padden FJ, Walter NM, Wyckoff HW. J Appl Phys 1959; 30:1485–8.
[4] Stocker W, Schumacher M, Graff S, Thierry A, Wittmann JC, Lotz B. Macromolecules 1998;31:807–14.
[5] Meille SV, Ferro DR, Bruckner S, Lovinger AJ, Padden FJ. Macromolecules 1994;27:2615–22.
[6] Lotz B, Kopp S, Dorset D. CR Acad Sci Ser II, Paris 1994;319: 187–92.
[7] Lotz B, Wittmann JC, Lovinger AJ. Polymer 1996;37:4979–92.
[8] Turner-Jones A, Cobbold AJ. J Polym Sci 1968;B6:539–46.
[9] Varga J. Mater Sci 1992;27:2557–79.
[10] Varga J. In: Polypropylene structure: blends and composites, vol. 1, 1995. p. 56–115 (chapter 3).
[11] Turner-Jones A, Aizlewood JM, Beckett DR. Makromol Chem 1964; 75:134–58.
[12] Padden Jr FJ, Keith HD. J Appl Phys 1959;30:1479–83.
[13] Fujiwara Y. Colloid Polym Sci 1975;253:273–82.
[14] Fillon B, Thierry A, Wittmann JC, Lotz B. J Polym Sci Polym Phys 1993;31:1407–24.
[15] Leugering HJ. Makromol Chem 1967;109:204.
[16] Garbarczyk J, Paukszta D. Colloid Polym Sci 1985;263:985–90.
[17] Hirsch JR, Wang PT. Texture Microstruct 1991;13:101–22.
[18] Pluta M, Bartczak Z, Galeski A. Polymer 2000;41:2271–88.
[19] Chu F, Yamaoko T, Kimura Y. Polymer 1995;36:2523–30.
[20] Li JX, Cheung WL. Polymer 1998;39:6935–40.
[21] Karger-Kocsis J, Varga J. J Appl Polym Sci 1996;62:291–300.
[22] Lotz B, Mathieu C, Thierry A, Lovinger AJ, De Rosa C, Ruiz de Ballesteros O, Auriemma F. Macromolecules 1998;31:9253–7.
[23] Aboulfaraj M, Ulrich B, Dahoun A, G'Sell C. Polymer 1993;34: 4817–25.
[24] Flory PJ, Yoon DY. Nature 1978;272:226–9.
[25] Clark ES. J Macromol Sci Phys 1967;1:795–800.
[26] Brown RG. J Chem Phys 1964;40:2900–9.
[27] Macturk KS, Eby RK, Farmer BL. Polymer 1996;37:4999–5003.
[28] Kimmig M, Strobl G, Stuhn B. Macromolecules 1994;27:2481–95.
[29] Takashi Y, Tetsuhiko H. Polymer 1986;27:986–92.
[30] Dobrovolnay-Marand E, Hsu SL, Shih CK. Macromolecules 1987;20: 1022–9.
[31] Schaefer D, Spiess HW, Suter UW, Fleming WW. Macromolecules 1990;23:3431–9.
[32] Rutledge GC, Suter UW. Macromolecules 1992;25:1546–53.
[33] Seguela R, Staniek E, Escaig B, Fillon B. J Appl Polym Sci 1999;71: 1873–85.
[34] Aboulfaraj M, G'Sell C, Ulrich B, Dahoun A. Polymer 1995;36: 731–42.

[35] Li JX, Cheung WL, Chan CM. Polymer 1999;40:3641–56.
[36] Arruda EM, Boyce MC. Polym Eng Sci 1990;30:1288–98.
[37] Karger-Kocsis. J Polym Eng Sci 1996;36:203–10.
[38] Arruda EM, Boyce MC, Jayachandran R. Mech Mater 1995;19: 193–212.
[39] Xu W, Arruda EM. Proceedings of Plasticity'99, Cancun, Mexico, January, 1999.
[40] Lima MFS, Vasconcellos MAZ, Samios D. J Polym Sci. Part B: Polym Phys 2002;40:896–903.
[41] Wang ZG, Hsiao BS, Srinivas S, Brown GM, Tsou AH, Cheng SZD, Stein RS. Polymer 2001;42:7561–6.
[42] Coulon G, Castelein G, G'Sell C. Polymer 1998;40:95–110.
[43] Mayo SL, Olafson BD, Goddard WA. J Phys Chem 1990;94: 8897–909.